# The observed variation in cloud-induced longwave radiation in response to sea surface temperature over the Pacific warm pool from MTSAT-1R imagery

Heeje Cho,[1] Chang-Hoi Ho,[1,2,3] and Yong-Sang Choi[3,4]

Received 14 June 2012; revised 10 August 2012; accepted 17 August 2012; published 22 September 2012.

[1] This study investigated variations in outgoing longwave radiation (OLR) in response to changes in sea surface temperature (SST) over the Pacific warm pool area (20°N–20°S, 130°E–170°W). OLR values were obtained from recent (January 2008–June 2010) geostationary window channel imagery at hourly resolution, which resolves processes associated with tropical convective clouds. We used linear regression analysis with the domain-averaged OLR and SST anomalies (i.e., $\Delta OLR$, $\Delta SST$; deviations from their 90-day moving averages). Results show that the regression slope appears to be significant only with SST least-affected by cloud radiative forcing, for which SST needs to be obtained as daily average over cloud-free regions ($\Delta SST_{clear}$). The estimated value of $\Delta OLR/\Delta SST_{clear}$ is 15.72 W m$^{-2}$ K$^{-1}$, indicating the presence of strong outgoing longwave radiation in response to surface warming. This atmospheric cooling effect is found to be primarily associated with reduced areal coverage of clouds ($-14.4\%$ K$^{-1}$). **Citation:** Cho, H., C.-H. Ho, and Y.-S. Choi (2012), The observed variation in cloud-induced longwave radiation in response to sea surface temperature over the Pacific warm pool from MTSAT-1R imagery, *Geophys. Res. Lett.*, *39*, L18802, doi:10.1029/2012GL052700.

## 1. Introduction

[2] In response to anomalous radiative forcing, changes in the global mean surface temperature depend largely on the strength of various radiative feedbacks. It is widely accepted that some of the most important, but highly uncertain feedbacks in the global climate system are those involving clouds. Clouds effectively regulate the Earth's top-of-atmosphere (TOA) radiation budget by reflecting solar insolation and trapping planetary infrared emissions; therefore, their response to surface temperature is of primary interest. Previous observational studies of cloud longwave (LW) influences on global warming varied widely [e.g., *Lindzen et al.*, 2001; *Stephens*, 2005; *Rondanelli and Lindzen*, 2008; *Zelinka and Hartmann*, 2010].

[3] One of major reasons for this uncertainty is that the cloud feedback "signal" is not strong enough to be distinguished from the "noise" due to cloud variation in the present observational data. In this context, cloud noise refers to the variations that are not feedbacks to surface temperature change. Over a short timescale, this noise tends to act as considerable radiative forcing, randomly changing surface temperature, whereas the cloud feedback signal is due to the radiative response of cloud to change in surface temperature. Obviously, this noise effect may bias estimations of the cloud feedback, and yet cannot be eliminated by usual mathematical filtering.

[4] As the cloud's non-feedback noise effect is mixed with cloud feedback processes in the observed records, this study attempts to separate the sea surface temperature (SST) variations caused by clouds and those that change clouds. Only the latter should be categorized as a cloud response to SST change. We will show that it may be possible to minimize the noise effect that exists in temporal variations in SST, by using cloud fraction information from high temporal resolution geostationary satellite data. Following previous studies on tropical cloud response to local SST changes [e.g., *Ramanathan and Collins*, 1991; *Horváth and Soden*, 2008; *Rondanelli and Lindzen*, 2008], we confined our analysis to the Pacific warm pool region (PWP; 20°N–20°S, 130°E–170°W). The clouds over the PWP are known to be the most sensitive to local SST change through convective processes [e.g., *Zhang*, 1993].

[5] Compared to detailed cloud property retrievals from satellites, radiative flux data are more directly associated with the issue of determining "radiative" feedback processes. Moreover, the large differences among the previous results on tropical cloud feedback may be related to highly uncertain cloud retrievals [e.g., *Choi et al.*, 2005; *Ohring et al.*, 2005; *Choi and Ho*, 2009]. For these reasons, we used the TOA longwave radiative fluxes that are calculated from satellite-observed radiances, as shown below.

## 2. Data and Method

[6] Estimation of cloud response to SST change should be supported by observations with a timescale that is short enough to resolve the cloud processes in the atmosphere. For the PWP analysis region, the lifetime of cloud process associated with cumulonimbus is known to range from hours to days. It is difficult to observe fast cloud processes from monthly data for SST and radiative flux. Thus, we try to concentrate on short-term variations at a timescale of less than a few days.

[7] Cloud variations in the PWP have been monitored hourly by the Japanese Multi-functional Transport Satellite

[1]Computational Science and Technology, Seoul National University, Seoul, South Korea.
[2]School of Earth and Environmental Sciences, Seoul National University, Seoul, South Korea.
[3]Center for Climate/Environment Change Prediction Research, Ewha Womans University, Seoul, South Korea.
[4]Department of Environmental Science and Engineering, Ewha Womans University, Seoul, South Korea.

Corresponding author: Y.-S. Choi, Department of Environmental Science and Engineering, Ewha Womans University, Daehyeon-dong, Seodaemun-gu, Seoul 120-750, South Korea. (ysc@ewha.ac.kr)


0094-8276/12/2012GL052700

(MTSAT-1R) on the geostationary orbit centered at 140°E. The window channel (centered at 11 $\mu$m) imagery of MTSAT-1R is useful to capture longwave variations due to changes in both clouds and surface temperature, because the effects of other factors, such as column-integrated water vapor and vertical structure of atmospheric temperature, barely interfere with radiance at that wavelength. The data period used is January 1, 2008 to June 30, 2010. The SST data is the National Oceanic and Atmospheric Administration's 0.25° daily optimum interpolation SST version 2, using microwave satellite measurements from the Advanced Microwave Scanning Radiometer and infrared satellite measurements from the Advanced Very High Resolution Radiometer [*Reynolds et al.*, 2007]. Unlike the near-all-weather coverage of microwave measurements, the infrared-based SSTs are obtained only over clear sky areas. This spatial inhomogeneity of the SST data between clear sky and cloudy sky may have influences as the observational noise, however, we focus on the physical noise effect.

[8] We calculated OLR values on a pixel basis ($\sim 4 \times 4$ km$^2$ resolution at nadir) of the MTSAT-1R dataset, as a third-order polynomial function of 11-$\mu$m radiance ($L_{11}$; equation (1)):

$$OLR = 44.95 + 50.97 L_{11} - 4.02 {L_{11}}^2 + 0.15 {L_{11}}^3, \qquad (1)$$

where the four constant coefficients of the polynomial function in equation (1) are obtained by a regression least-square fit of OLRs against $L_{11}$ simulated by a radiative transfer model with various environmental conditions; each of the 840 simulations incorporates every combination of 7 satellite zenith angles (0°–60°, 10° interval), 8 cloud top heights (2–16 km, 2 km interval), and 15 cloud optical thicknesses (20–48, 2 interval). For the radiative transfer simulations, the discrete ordinates radiative transfer (DISORT) model "Santa Barbara DISORT Atmospheric Radiative Transfer" (SBDART) [*Ricchiazzi et al.*, 1998] is used. The root-mean-square difference between $L_{11}$-inferred OLRs and OLRs measured directly from broadband satellite instruments is known to be less than approximately 10 W m$^{-2}$ [*Ohring et al.*, 1984; *Ba et al.*, 2003]. The bias of $L_{11}$-inferred OLR may stem largely from water vapor because $L_{11}$ does not involve absorption by water vapor, but by cloud particles and surface. Therefore, it should be noted that our OLR only represents longwave variations induced by cloud and surface properties by excluding the other infrared channels of MTSAT-1R in OLR calculations. Other biases due to instrumentation factors, algorithms, etc. are also relevant for estimation of feedback, and they may eventually reduce the statistical significance of the regression (e.g., coefficient of determination: $R^2$). In many previous studies, $R^2$ between SST and OLR was found to be very low in monthly-observed data.

[9] A single-channel threshold test using 11-$\mu$m channel-brightness temperature ($BT_{11}$) is employed to determine the presence of cloud at each pixel in the MTSAT-1R data. As most opaque clouds represented in the longwave radiation can be distinguished by this $BT_{11}$ test [e.g., *Rossow and Garder*, 1993; *Choi et al.*, 2005; *Horváth and Soden*, 2008], many previous cloud studies using geostationary observations have employed the single-channel test for identification of cloudy pixels. As discussed later, the present study tested various threshold values for $BT_{11}$, and the major conclusion in this study was found to be robust and remained unchanged, regardless of the threshold values within a certain range.

[10] We generate daily SST and OLR time series that are area-averaged over the PWP, but for selective cases of cloud conditions. The detailed methodology for generating the time series is given by equations (2a) to (4c):

$$A^{hour}_{clous}(i) = \frac{\sum_{m}^{cloudy \cap (i)} \cos^{-1}\theta_m}{\sum_{m}^{i} \cos^{-1}\theta_m} \qquad (2a)$$

$$A^{day}_{cloud}(i) = \sum_{hour=0}^{23} \frac{A^{hour}_{cloud}(i)}{24} \qquad (2b)$$

$$\overline{SST}^{day}_{entire} = \sum_{i}^{PWP} SST^{day}(i) \cdot \cos\phi_i \Big/ \sum_{i}^{PWP} \cos\phi_i \qquad (3a)$$

$$\overline{SST}^{day}_{cloud} = \sum_{i}^{PWP} SST^{day}(i) A^{day}_{cloud}(i) \cdot \cos\phi_i \Big/ \sum_{i}^{PWP} A^{day}_{cloud}(i) \cdot \cos\phi_i \qquad (3b)$$

$$\overline{SST}^{day}_{clear} = \sum_{i}^{PWP} SST^{day}(i) \cdot A^{day}_{clear}(i) \cdot \cos\phi_i \Big/ \sum_{i}^{PWP} A^{day}_{clear}(i) \cdot \cos\phi_i \qquad (3c)$$

$$\overline{OLR}^{day}_{entire} = \frac{1}{24} \cdot \sum_{hour=0}^{23} \left\{ \sum_{m}^{PWP} OLR^{hour}(m) \cdot \cos^{-1}\theta_m \Big/ \sum_{m}^{PWP} \cos^{-1}\theta_m \right\} \qquad (4a)$$

$$\overline{OLR}^{day}_{cloud} = \frac{1}{24} \cdot \sum_{hour=0}^{23} \left\{ \sum_{m}^{cloudy \cap PWP} OLR^{hour}(m) \cdot \cos^{-1}\theta_m \Big/ \sum_{m}^{cloudy \cap PWP} \cos^{-1}\theta_m \right\} \qquad (4b)$$

$$\overline{OLR}^{day}_{clear} = \frac{1}{24} \cdot \sum_{hour=0}^{23} \left\{ \sum_{m}^{clear \cap PWP} OLR^{hour}(m) \cdot \cos^{-1}\theta_m \Big/ \sum_{m}^{clear \cap PWP} \cos^{-1}\theta_m \right\} \qquad (4c)$$

where $i$ indicates the $i$-th SST grid; $m$ the $m$-th MTSAT-1R pixel (with spatial resolution of $\sim 4 \times 4$ km$^2$ at nadir); $\theta$ the satellite zenith angle; $\phi$ the latitude; $\cap$ the intersection of two sets. As $\cos^{-1}\theta$ is proportional to the size of MTSAT-1R pixel, we calculate an hourly cloud fraction of each $i$-th 0.25° SST grid $A^{hour}_{cloud}(i)$ via equation (2a), using cloudy pixels within the grid. A daily cloud fraction of each SST grid, $A^{day}_{cloud}(i)$ is calculated by simple time averages (equation (2b)). Note that in the results, different threshold values were used for 'cloudy' pixel detection ($BT_{11} < 270$ K) and 'clear' pixel detection ($BT_{11} \geq 280$ K), so that $A^{day}_{cloud}(i) + A^{day}_{clear}(i) < 1$. Over the PWP, $BT_{11}$ values between 270 K and 280 K are generally regarded as the cloudy-sky signal, but

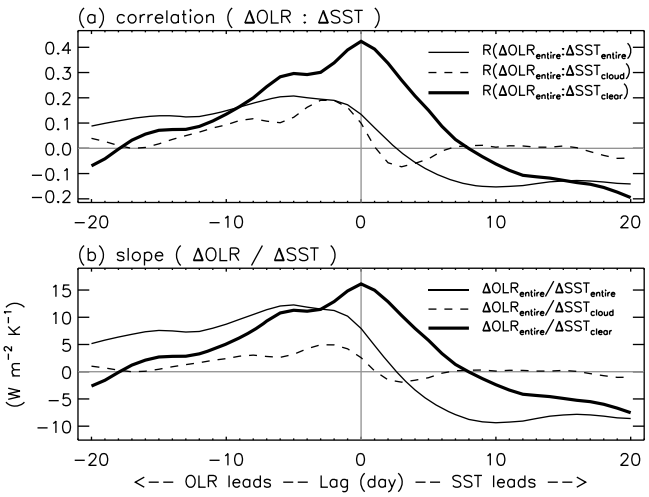


**Figure 1.** Lagged linear (a) correlations and (b) regression slopes between $\Delta OLR_{\text{entire}}$ and $\Delta SSTs$. Positive abscissa value indicates that $\Delta SSTs$ lead $\Delta OLR_{\text{entire}}$. $\Delta SSTs$ are the anomalies against the area-averaged SSTs over the entire domain of analysis (thin solid), cloudy area (dashed), and clear-sky area (thick solid).

the range can be avoided to eliminate ambiguity of cloud masking. During the study period, $A_{cloud}^{dayr}(i)$ varies between 5% and 35% (standard deviation 4.9%), and $A_{clear}^{day}(i)$ varies between 41% and 86% (standard deviation 7.7%).

[11] The daily SST and OLR time series are then calculated by equations (3) and (4), respectively. $\overline{SST}_{entire}^{day}$ is the daily average of SSTs in the PWP (equation (3a)), while $\overline{SST}_{cloud}^{day}$ is the cloud-weighted average of SSTs in the PWP (equation (3b)). The weighting factors in equations (3b) and (3c) are proportional to the daily cloud and clear coverage, respectively. For instance, in equation (3b), the weighting factor would be 1 for a grid where all pixels are overcast in a day, and 0.5 where half the pixels are overcast in a day. Calculation of $\overline{SST}_{clear}^{day}$ values follows the consistent rule (equation (3c)). Cosine values are multiplied with due consideration of the size of each MTSAT-1R pixel or SST grid. As the temporal resolution of SST data is lower than that of MTSAT-1R OLR, temporal degradation of OLR is also unavoidable in order to compare with SST data; daily OLR values are averaged from 00:00 UTC to 23:00 UTC (equation (4)).

[12] To remove low-frequency variations whose timescales are considered to be longer than that of tropical cloud processes, the daily $\overline{OLR}_x^{day}$ and $\overline{SST}_x^{day}$ ($x$ = entire, cloud, or clear) anomalies ($\Delta OLR_x$ and $\Delta SST_x$) are calculated by subtracting their moving average values with a 90-day centered smoother, which effectively isolates short timescale fluctuations [e.g., *Zhang et al.*, 1995]. The smoother also filters out the annual-cycle climatology, which is difficult to obtain from data series of less than three years. The choice of the 90-day smoother is to remove seasonality, but not to remove meaningful 1–3 month fluctuations associated with dynamics. Nevertheless, the change of the smoother length within 30–90 days does not affect the main conclusion of this study. We expect that the variations in both $\Delta SST_{\text{entire}}$ and $\Delta SST_{\text{cloud}}$ are more influenced by radiative forcings (mostly associated with cloud changes), than that of $\Delta SST_{\text{clear}}$ (equation (3c)). It is noted that extraction of $\Delta SST_{\text{clear}}$ is allowed only using hourly clear-sky detection from geostationary satellites, such as the MTSAT-1R data used in this study.

[13] Linear regression slopes ($\Delta OLR/\Delta SST$) are calculated for each set of anomalous $\Delta OLR$ and $\Delta SST$ time series. To overcome the limitation of linear regression slope in determining causality between OLR and SST, we also examined the cross-correlation coefficients for different time lags between $\Delta OLR$ and $\Delta SST$. For comparison with results from daily data, the monthly-mean $\Delta OLR_x$ and $\Delta SST_x$ values are also calculated by simple time-averaging.

## 3. Observed Response of OLR and Cloudiness to SST Change Over the PWP

[14] Initially, the instantaneous (coincident) relationship between $\Delta OLR_{\text{entire}}$ and $\Delta SST_{\text{entire}}$ was calculated on daily and monthly timescales. The linear regression slope ($\Delta OLR_{\text{entire}}/\Delta SST_{\text{entire}}$) from monthly data was $4.20 \pm 5.84$ W m$^{-2}$ K$^{-1}$ (mean $\pm$ standard error). As the regression slope is greater than the Planck response of longwave emission (3.3 W m$^{-2}$ K$^{-1}$), the obtained slope may imply that the Earth's climate has a slight longwave cooling effect for increased SST. This result is consistent with most previous studies using monthly-mean data [e.g., *Lindzen and Choi*, 2009], but raises concerns about the wide uncertainty range of the slope, mostly owing to the small sample size. Interestingly, using daily-mean data, we found much higher regression slope ($\Delta OLR_{\text{entire}}/\Delta SST_{\text{entire}} = 8.31 \pm 1.76$ W m$^{-2}$ K$^{-1}$), implying strong release of longwave radiation for increased SST.

[15] The positive correlation between $\Delta OLR_{\text{entire}}$ and $\Delta SST_{\text{entire}}$ would not only be a consequence of SST-induced OLR change, but also of OLR-induced SST change. That is to say, it is feasible that the strong positive correlation would be induced solely by SST contaminated by non-feedback cloud noise. For instance, it is natural that the decrease in cloud fraction leads to the increase in SST by allowing greater solar heating of the surface; at the same time, OLR would increase owing to warmer emission temperature (i.e., more infrared emission from the surface). Hence, the process finally gives positive correlation between OLR and SST. However, as mentioned, unless the increased SST eventually affects clouds, this does not represent feedbacks between SST and cloud.

[16] The non-feedback cloud process may often occur over the PWP region, and may readily prevent appropriate interpretation of the regression slope relevant to the radiative feedback strength. Therefore, it is necessary to investigate how the cross-correlation coefficient changes according to the time lag between OLR and SST, in order to get a better idea of whether the regression slope at zero lag is representative of radiative feedback strength, i.e., OLR change induced solely by SST change. Figure 1 shows the cross-regression between daily-mean $\Delta OLR$ and $\Delta SST$, where negative lag indicates that OLR leads SST; positive lag indicates that SST leads OLR. It is known that, in the case that OLR leads SST, the maximum $R^2$ tends to appear at negative lag, and $R^2$ at zero lag tends to be non-significant [*Spencer and Braswell*, 2010]. This case is seen in Figure 1a; the maximum $R^2$ between $\Delta OLR_{\text{entire}}$ and $\Delta SST_{\text{entire}}$ (thin

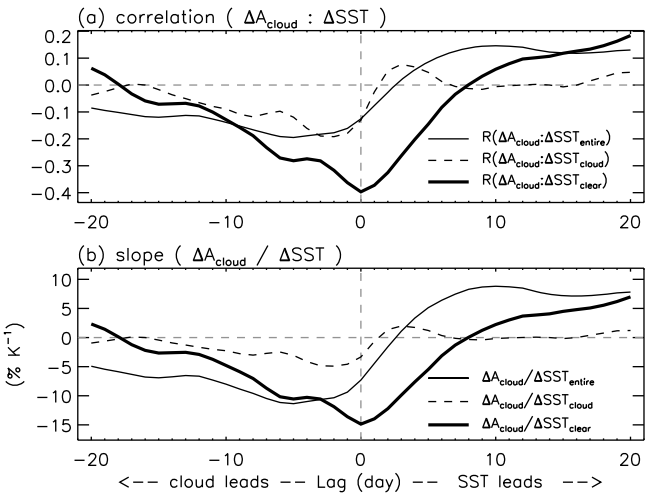


**Figure 2.** The same as Figure 1 but for $\Delta A_{\mathrm{cloud}}$ versus $\Delta SST$s.

solid line) is observed for a lag of approximately minus-5 days, and the value of $R^2$ decreases with increasing time lag, indicating that longwave radiative forcing affects SST. This effect is more evident for the further analysis with $\Delta SST_{\mathrm{cloud}}$, which is expected to be more strongly influenced than $\Delta SST_{\mathrm{entire}}$ by cloud radiative forcing. The corresponding cross-correlation coefficient between $\Delta OLR_{\mathrm{entire}}$ and $\Delta SST_{\mathrm{cloud}}$ is represented by the dashed line in Figure 1a, showing that the OLR–SST relationship is almost uncorrelated at around zero lag, similarly to the case with $\Delta SST_{\mathrm{entire}}$.

[17] However, OLR variations in response to SST are revealed by comparison of $\Delta SST$ with preceding (or at least coincident) $\Delta OLR$ (i.e., at zero or positive lags). Interestingly, unlike the analysis with $\Delta SST_{\mathrm{entire}}$ and $\Delta SST_{\mathrm{cloud}}$, the maximum $R^2$ between $\Delta OLR_{\mathrm{entire}}$ and $\Delta SST_{\mathrm{clear}}$ at zero lag appears as the top of the convex shape in the graph (thick solid line in Figure 1a). The value of $\Delta OLR_{\mathrm{entire}}/\Delta SST_{\mathrm{clear}}$ at zero lag is $15.72 \pm 1.02$ W m$^{-2}$ K$^{-1}$ (thick solid line in Figure 1b). It is known that this convex shape in the lead–lag relationship gives the desired signal of the cloud response to SST change from the regression slope at "zero" lag [e.g., *Frankignoul et al.*, 1998; *Lindzen and Choi*, 2011] once ignoring the possibility that the feedback effect can be delayed by ocean/atmosphere processes. This convex shape, however, would not occur with strong cloud contamination of the SST variation data [*Lindzen and Choi*, 2011]. We note that, for monthly data, the results ($\Delta OLR_{\mathrm{entire}}/\Delta SST_{\mathrm{clear}}$) do not show the convex shape. This may be because monthly $\Delta OLR_{\mathrm{entire}}/\Delta SST_{\mathrm{clear}}$ allows various processes at different timescales that may contaminate the signal of the exact cloud response to SST change.

[18] It is also worth examining whether $\Delta SST_{\mathrm{clear}}$ is physically meaningful in relation to tropical cloud processes. Taking clear-sky SST, however, does not exactly mean that we only consider SSTs outside of convection. This is because clear-sky SST at time $t$ can also be SST below clouds at time $t + 1$. Strong correlation between $\Delta SST_{\mathrm{entire}}$ and $\Delta SST_{\mathrm{clear}}$ (R = 0.73) assures that $\Delta SST_{\mathrm{clear}}$ can also represent essentially the SST variability over the PWP. Fundamentally, the role of dynamics is to reduce horizontal variations in SST. Convection, by contrast, increases horizontal variations in SST, de-correlating $\Delta SST_{\mathrm{entire}}$ and $\Delta SST_{\mathrm{clear}}$. To clarify this, we separated the SST anomalies into low- and high frequency data with a 7-day centered smoother. The correlation between the low-frequency $\Delta SST_{\mathrm{entire}}$ and $\Delta SST_{\mathrm{clear}}$ is higher (R = 0.77) than that between the high-frequency $\Delta SST_{\mathrm{entire}}$ and $\Delta SST_{\mathrm{clear}}$ (R = 0.51). This suggests that the time scale of dynamics is longer than that of convection over the PWP. $\Delta SST_{\mathrm{clear}}$ indeed contains intrinsic dynamics over the PWP, but with reduced cloud noise effects.

[19] Despite the strong correlation between $\Delta SST_{\mathrm{entire}}$ and $\Delta SST_{\mathrm{clear}}$, $\Delta SST_{\mathrm{entire}}$ and $\Delta SST_{\mathrm{clear}}$ (as well as $\Delta SST_{\mathrm{cloud}}$ and $\Delta SST_{\mathrm{clear}}$) have remarkably different lead–lag relationships with $\Delta OLR_{\mathrm{entire}}$. This provides an important reason why the slope $\Delta OLR_{\mathrm{entire}}/\Delta SST_{\mathrm{clear}}$ is not an artifact of uneven horizontal distribution of SST field over the PWP. If the slopes were artifacts from the SST field, then the lead–lag relationship between $\Delta OLR_{\mathrm{entire}}$-$\Delta SST_{\mathrm{cloud}}$ would be similar to that of $\Delta OLR_{\mathrm{entire}}$-$\Delta SST_{\mathrm{clear}}$ because $\Delta SST_{\mathrm{clear}}$ and $\Delta SST_{\mathrm{cloud}}$ would only reflect the variations in cloud coverage. Thus, we used $\Delta SST_{\mathrm{clear}}$ as the noise-reduced SST that can correctly indicate the magnitude of forcing that changes clouds.

[20] In order to examine how clouds are involved in OLR variations, we further investigated the OLR variability in association with clouds by separation of cloudy-sky OLR and clear-sky OLR. The OLR variations are regulated mostly by the longwave emission, especially from clouds and the Earth's surface, because the OLR is inferred from 11 $\mu$m radiation only. Beside the contribution of the surface to the variation in OLR via the Planck response, the variation in OLR is regarded as a function of (1) cloud-top temperature ($T_{\mathrm{cloud}}$), and (2) horizontal coverage of clouds ($A_{\mathrm{cloud}}$). The $T_{\mathrm{cloud}}$ mainly determines $OLR_{\mathrm{cloud}}$ which calculation is confined within cloudy-sky area only, while both $T_{\mathrm{cloud}}$ and $A_{\mathrm{cloud}}$ determine $OLR_{\mathrm{entire}}$. Our cross-correlation analysis between $\Delta OLR_{\mathrm{cloud}}$ and $\Delta SST_{\mathrm{clear}}$ indicates that cloud thermal emission associated with $T_{\mathrm{cloud}}$ is uncorrelated with the variation in SST (not shown in the figure). This potentially supports the hypothesis that the cloud top temperature is insensitive to SST [*Hartmann and Larson*, 2002].

[21] More importantly, $\Delta A_{\mathrm{cloud}}$ and $\Delta SST_{\mathrm{clear}}$ had significant negative correlation with its minimum peak of cross-correlation coefficient at zero lag (thick solid line in Figure 2a); the corresponding regression slope, $\Delta A_{\mathrm{cloud}}/\Delta SST_{\mathrm{clear}}$ is $-14.4 \pm 1.0\%$ K$^{-1}$ (thick solid line in Figure 2b). In this case, the convex shape with a peak at zero lag is revealed, confirming the validity of the slope. Of course, this shape does not appear when using cloud-affected SST anomalies, $\Delta SST_{\mathrm{entire}}$ and $\Delta SST_{\mathrm{cloud}}$. $\Delta A_{\mathrm{cloud}}/\Delta SST_{\mathrm{entire}}$ (and $\Delta A_{\mathrm{cloud}}/\Delta SST_{\mathrm{cloud}}$) is negative at negative lag, and becomes positive at positive lag. This probably results because increased $A_{\mathrm{cloud}}$ cools the SST owing to the cloud dimming effect. Consequently, the result of $\Delta A_{\mathrm{cloud}}$ (Figure 2) is very consistent with that of $\Delta OLR_{\mathrm{entire}}$ (Figure 1).

[22] As mentioned in the previous section, these results are based on the $BT_{11}$ threshold value of 280 K for clear-sky pixel detection. To check the dependence of the result on the choice of the threshold, we applied various threshold values between 270 K and 290 K for clear-sky pixel detection. Irrespective of the selected threshold, the convex shape of the correlation with respect to time lag was maintained. If this threshold is less than 270 K (allowing excessively larger clear-sky area), the maximum $R^2$ between $\Delta OLR_{\mathrm{entire}}$ and

**Table 1.** The Value ± Standard Errors of $\Delta OLR_{\text{entire}}/\Delta SST_{\text{clear}}$ and $\Delta A_{\text{cloud}}/\Delta SST_{\text{clear}}$ From Simple Linear Regression With Different $BT_{11}$ Thresholds for Clear-Sky/Cloudy Pixel Detection[a]

| Variables | Clear-Sky Detection Test | | |
|---|---|---|---|
| | $BT_{11} \geq 270$ K | $BT_{11} \geq 280$ K | $BT_{11} \geq 290$ K |
| $\Delta OLR_{\text{entire}}/\Delta SST_{\text{clear}}$, $\text{Wm}^{-2}\text{K}^{-1}$ | $16.63 \pm 1.19$ | $15.72 \pm 1.02$ | $11.76 \pm 0.77$ |
| | $(39.37 \pm 1.14)$ | $(34.53 \pm 1.00)$ | $(25.80 \pm 0.74)$ |
| $\Delta A_{\text{cloud}}(BT_{11} < 270\text{ K})/\Delta SST_{\text{clear}}$, $\%\ \text{K}^{-1}$ | $-15.1 \pm 1.2$ | $-14.4 \pm 1.0$ | $-11.0 \pm 0.8$ |
| | $(-38.7 \pm 1.1)$ | $(-34.0 \pm 1.0)$ | $(-25.4 \pm 0.7)$ |
| $\Delta A_{\text{cloud}}(BT_{11} < 260\text{ K})/\Delta SST_{\text{clear}}$, $\%\ \text{K}^{-1}$ | $-12.3 \pm 0.9$ | $-11.6 \pm 0.8$ | $-8.8 \pm 0.6$ |
| | $(-30.2 \pm 0.9)$ | $(-26.4 \pm 0.8)$ | $(-19.8 \pm 0.6)$ |

[a]All the anomaly values are daily means. The results from the reduced major axis method are shown in parentheses.

$\Delta SST_{\text{clear}}$ shifts to negative lags, implying that the influence of OLR on $\Delta SST_{\text{clear}}$ becomes important. The slopes at zero lag for the thresholds of 270, 280, and 290 K are shown in Table 1. It is shown that, for more rigorous threshold for clear-sky detection, the value of $\Delta OLR_{\text{entire}}/\Delta SST_{\text{clear}}$ is lower. This may result from less sampling of clear-sky SSTs, as well as from excluding more of the influence of cloud on SST.

[23] On the other hand, for thermally colder clouds with $BT_{11} < 260$ K, $\Delta A_{\text{cloud}}/\Delta SST_{\text{clear}}$ was smaller by $\sim$3% $\text{K}^{-1}$ compared to the cloud with $BT_{11} < 270$ K, irrespective of clear-sky SST. This implies that relatively thin clouds (corresponding to $\text{BT}_{11}$ between 260 K and 270 K) would decrease by $\sim$3% $\text{K}^{-1}$. Table 1 also shows the results from the reduced major axis (RMA) method (the numbers in parentheses), which is known to be more appropriate for relating two co-dependent variables, or for an independent variable that includes errors [*Smith*, 2009]. We note that a slope from simple linear regression may bias toward zero value, in comparison to the RMA method. Although this RMA gives more intensified slopes without changing the sign, the different slopes obtained from different statistical approaches is an issue to be addressed; however, this is beyond the scope of the present paper.

[24] *Lindzen et al.* [2001] also used geostationary satellite observations, and demonstrated significant reduction in cloud coverage with increasing SST over the similar analysis region. It is noted that Lindzen et al. hypothesized that proper estimation of the cloud feedback essentially requires normalization by "cumulus area" to distinguish changes in the amount of convection from changes in detrainment per unit convection. The cumulus area, as defined by Lindzen et al., can be extracted by $BT_{11} < 220$ K. Based on this definition, we also examined the response of the cumulus area to SST change (i.e., $\Delta A_{\text{cloud}}(BT_{11} < 220\text{ K})/\Delta SST_{\text{clear}}$). However, we find neither a significant change in cumulus area nor a robust quantity owing to the distorted shape of cross-correlation. This is possibly because we related the cumulus area with the SST anomaly, not with the 'absolute value' of SST that actually affects the cumulus area. We also suspect that most of the PWP is occupied by convection, and the amount of convection remains relatively constant with little influence of moisture convergence into or out of the PWP. Despite all these possibilities associated with normalization, the cloud shrinkage is evident in this study without any normalization procedure [e.g., *Lindzen et al.*, 2001; *Rapp et al.*, 2005]. Beside the issue of the normalization effect, this study suggests that the analysis by *Lindzen et al.* [2001] and subsequent studies [e.g., *Lin et al.*, 2002; *Choi et al.*, 2005] would remain unsatisfactory, in that they have examined only coincident relations between cloud and SST. Moreover, their cloud-weighted SST is similar to $SST_{\text{cloud}}$ defined in this study, which, as we demonstrated, can bring about differing interpretation of cloud response to SST change.

## 4. Summary and Discussion

[25] It is important to better understand the longwave response to surface temperature change in order to infer tropical longwave feedback. Here, we focused on the short-term longwave response of cloud over the PWP using observations of geostationary satellite TOA longwave radiation and SST. We have shown that great care is needed when interpreting linear regression slopes of OLR and SST. This study demonstrates that clouds always have a strong influence on SST variations, and consequently there is potential underestimation of cloud response to SST change when using unfiltered cloud-contaminated SST data. In addition, for successful extraction of noise-reduced SST forcing, short-timescale data is necessary. Perhaps geostationary satellite observation may be the most helpful measurement to achieve this.

[26] The linear regression slope of OLR and SST ($\Delta OLR_{\text{entire}}/\Delta SST_{\text{entire}}$) differs according to the timescale: $4.20 \pm 5.84$ W $\text{m}^{-2}$ $\text{K}^{-1}$ for monthly-mean data, and $8.31 \pm 1.76$ W $\text{m}^{-2}$ $\text{K}^{-1}$ for daily-mean data. We also used $SST_{\text{clear}}$ (noise-reduced SST), and obtained the slope, $\Delta OLR_{\text{entire}}/\Delta SST_{\text{clear}} = 15.72 \pm 1.02$ W $\text{m}^{-2}$ $\text{K}^{-1}$. This value was obtained by zero-lag regression slope of OLR on SST with maximum correlation at zero lag, which accurately represents longwave response to SST change. This cooling effect is found to be primarily associated with the shrinkage of the areal coverage of clouds (about $-14.4 \pm 1.0\%$ $\text{K}^{-1}$).

[27] Despite the importance of this issue in reducing the uncertainty of climate prediction, it should be noted that our results in the PWP do not directly indicate climate sensitivity or total cloud feedback on the global scale. As to climate sensitivity, the strong cooling effects of clouds over this region may be reduced once scaled globally. As to total cloud feedback, possible longer-term feedbacks may be present in association with other meteorological elements and large-scale dynamics with long-term persistence. In addition, positive shortwave (albedo) feedback would be expected owing to shrinkage of cloud coverage, and this might offset longwave feedback [*Zelinka and Hartmann*, 2011]. The shortwave cloud feedback involves the response of optical properties of clouds [*Chang and Coakley*, 2007]. It would be useful to employ our proposed methodology to verify these previous findings.

[28] **Acknowledgments.** This study is supported by the Basic Science Research Program through the National Research Foundation of Korea (NRF), funded by the Ministry of Education, Science and Technology (2012-0000857). This study is also supported by Korea Minister of Environment as "The Eco-technopia 21 project". We thank Richard S. Lindzen, Roberto Rondanelli, and Sukyoung Lee for valuable comments.

[29] The Editor thanks Roberto Rondanelli and Richard Lindzen for assisting in the evaluation of this paper.

## References

Ba, M. B., R. G. Ellingson, and A. Gruber (2003), Validation of a technique for estimating OLR with the GOES sounder, *J. Atmos. Oceanic Technol.*, *20*, 79–89, doi:10.1175/1520-0426(2003)020<0079:VOATFE>2.0.CO;2.

Chang, F.-L., and J. A. Coakley (2007), Relationships between marine stratus cloud optical depth and temperature: Inferences from AVHRR observations, *J. Clim.*, *20*, 2022–2036, doi:10.1175/JCLI4115.1.

Choi, Y.-S., and C.-H. Ho (2009), Validation of the cloud property retrievals from the MTSAT-1R imagery using MODIS observations, *Int. J. Remote Sens.*, *30*, 5935–5958, doi:10.1080/01431160902791887.

Choi, Y.-S., C.-H. Ho, and C.-H. Sui (2005), Different optical properties of high cloud in GMS and MODIS observations, *Geophys. Res. Lett.*, *32*, L23823, doi:10.1029/2005GL024616.

Frankignoul, C., A. Czaja, and B. L'Heveder (1998), Air–sea feedback in the north Atlantic and surface boundary conditions for ocean models, *J. Clim.*, *11*, 2310–2324, doi:10.1175/1520-0442(1998)011<2310:ASFITN>2.0.CO;2.

Hartmann, D. L., and K. Larson (2002), An important constraint on tropical cloud–climate feedback, *Geophys. Res. Lett.*, *29*(20), 1951, doi:10.1029/2002GL015835.

Horváth, Á., and B. J. Soden (2008), Lagrangian diagnostics of tropical deep convection and its effect upon upper-tropospheric humidity, *J. Clim.*, *21*, 1013–1028, doi:10.1175/2007JCLI1786.1.

Lin, B., B. Wielicki, L. H. Chambers, Y. Hu, and K.-M. Xu (2002), The iris hypothesis: A negative or positive cloud feedback?, *J. Clim.*, *15*, 3–7, doi:10.1175/1520-0442(2002)015<0003:TIHANO>2.0.CO;2.

Lindzen, R. S., and Y.-S. Choi (2009), On the determination of climate feedbacks from ERBE data, *Geophys. Res. Lett.*, *36*, L16705, doi:10.1029/2009GL039628.

Lindzen, R. S., and Y.-S. Choi (2011), On the observational determination of climate sensitivity and its implications, *Asia Pac. J. Atmos. Sci.*, *47*, 377–390, doi:10.1007/s13143-011-0023-x.

Lindzen, R. S., M.-D. Chou, and A. Y. Hou (2001), Does the Earth have an adaptive infrared iris?, *Bull. Am. Meteorol. Soc.*, *82*, 417–432, doi:10.1175/1520-0477(2001)082<0417:DTEHAA>2.3.CO;2.

Ohring, G., A. Gruber, and R. G. Ellingson (1984), Satellite determination of the relationship between total longwave flux and infrared window radiance, *J. Appl. Meteorol.*, *23*, 416–425, doi:10.1175/1520-0450(1984)023<0416:SDOTRB>2.0.CO;2.

Ohring, G., B. Wielicki, R. Spencer, B. Emery, and R. Datla (2005), Satellite instrument calibration for measuring global climate change: Report of a workshop, *Bull. Am. Meteorol. Soc.*, *86*, 1303–1313, doi:10.1175/BAMS-86-9-1303.

Ramanathan, V., and W. Collins (1991), Thermodynamic regulation of ocean warming by cirrus clouds deduced from observations of the 1987 El Niño, *Nature*, *351*, 27–32, doi:10.1038/351027a0.

Rapp, A. D., C. Kummerow, W. Berg, and B. Griffith (2005), An evaluation of the proposed mechanism of the adaptive infrared iris hypothesis using TRMM VIRS and PR measurements, *J. Clim.*, *18*, 4185–4194, doi:10.1175/JCLI3528.1.

Reynolds, R. W., T. M. Smith, C. Liu, D. B. Chelton, K. S. Casey, and M. G. Schlax (2007), Daily high-resolution-blended analyses for sea surface temperature, *J. Clim.*, *20*, 5473–5496, doi:10.1175/2007JCLI1824.1.

Ricchiazzi, P., S. Yang, C. Gautier, and D. Sowle (1998), SBDART: A research and teaching software tool for plane-parallel radiative transfer in the Earth's atmosphere, *Bull. Am. Meteorol. Soc.*, *79*, 2101–2114, doi:10.1175/1520-0477(1998)079<2101:SARATS>2.0.CO;2.

Rondanelli, R., and R. S. Lindzen (2008), Observed variations in convective precipitation fraction and stratiform area with sea surface temperature, *J. Geophys. Res.*, *113*, D16119, doi:10.1029/2008JD010064.

Rossow, W. B., and L. C. Garder (1993), Cloud detection using satellite measurements of infrared and visible radiances for ISCCP, *J. Clim.*, *6*, 2341–2369, doi:10.1175/1520-0442(1993)006<2341:CDUSMO>2.0.CO;2.

Smith, R. J. (2009), Use and misuse of the reduced major axis for line-fitting, *Am. J. Phys. Anthropol.*, *140*, 476–486, doi:10.1002/ajpa.21090.

Spencer, R. W., and W. D. Braswell (2010), On the diagnosis of radiative feedback in the presence of unknown radiative forcing, *J. Geophys. Res.*, *115*, D16109, doi:10.1029/2009JD013371.

Stephens, G. L. (2005), Cloud feedbacks in the climate system: A critical review, *J. Clim.*, *18*, 237–273, doi:10.1175/JCLI-3243.1.

Zelinka, M. D., and D. L. Hartmann (2010), Why is longwave cloud feedback positive?, *J. Geophys. Res.*, *115*, D16117, doi:10.1029/2010JD013817.

Zelinka, M. D., and D. L. Hartmann (2011), The observed sensitivity of high clouds to mean surface temperature anomalies in the tropics, *J. Geophys. Res.*, *116*, D23103, doi:10.1029/2011JD016459.

Zhang, C. (1993), Large-scale variability of atmospheric deep convection in relation to sea surface temperature in the tropics, *J. Clim.*, *6*, 1898–1913, doi:10.1175/1520-0442(1993)006<1898:LSVOAD>2.0.CO;2.

Zhang, G. J., V. Ramanathan, and M. J. McPhaden (1995), Convection-evaporation feedback in the equatorial Pacific, *J. Clim.*, *8*, 3040–3051, doi:10.1175/1520-0442(1995)008<3040:CEFITE>2.0.CO;2.